Dynamic Modelling and Aeroelastic Analysis of Rotor System using CFD Code & ADAMS Package

Dr. B. H. Ahn
Aerospace R&D Center
Daewoo Heavy Industries Ltd.
Taejeon, Korea

Prof. D. H. Lee
Department of Aerospace Engineering
Seoul National University
Seoul, Korea

Abstract

Exact prediction of performance and dynamic characteristic of helicopter rotor system is difficult because a blade is inherently flexible and the wake effect from preceding blades is dominant. In this research, developing three dimensional CFD method including wake analysis for aerodynamic loads computation, and using ADAMS package in structural dynamic analysis, new aeroelastic analysis method is developed. This method is applied to rotor system in hover and forward flight, so aerodynamic loads, blade deformations and aeroelastic stability are computed. Also, using graphic simulation capability of ADAMS, image rendering and animation of rotor system motion are performed. It is shown that, using methodology described herein, more accurate predictions are possible.

Introduction

Rotor blade has large elastic motion such as flap bending, lead-lag bending and torsional deflections because of high aspect ratio for stability and controllability. And rotor blade rotates under the influence of the wake from the preceding blades, thus unsteady phenomena including noise and vibration problem are occurred. So complex aeroelastic analysis considering the interaction of the wake, structural dynamics and aerodynamics is required to get the exact prediction of flowfields and vibrational characteristics. Aerodynamicists have performed their researches for rigid blade model without complex aeroelastic analysis including structural dynamic motion,[1-11] and in structural dynamic analysis, the suggested aeroelastic models rely on simpler representation for aerodynamic analysis.[12-26] Thus more complex modeling of the unsteady aerodynamic loads is required for accurate calculation of aeroelastic response and stability. Recently, combined method with complex aeroelastic calculation through Euler/Navier-Stokes equations is tried in limited case.[27]

In present research, developing three dimensional CFD (Computational Fluid Dynamics) method including wake analysis for aerodynamic loads computation, and using ADAMS (Automatic Dynamic Analysis of Mechanical Systems) in structural dynamic analysis, new aeroelastic analysis method is presented. Also, because aeroelastic phenomena of rotor blades have influence on vibrational characteristics of whole rotor system, developed method is not limited to rotor blade analysis, but performs analysis on rotor system including rotor blades, rotor

hub system and swashplate pitch control system. For this, multibody system modelling including moving parts and hinges, is performed using ADAMS. In this approach, geometrically nonlinear beam models are used to account for the various nonlinear structural coupling of rotor blade, and the global/local coordinate transformation technique is used to calculate aerodynamic forces of deformed rotor blades in three dimensional grid system. Thus, current work is distinguished from previous works in the following features :

1) Combined method through modulization and functional decomposition of analysis technique on aerodynamics (CFD code) and structural dynamics (ADAMS package).
2) Modeling and analysis of rotor system including rotor blades, rotor hub system and swashplate pitch control system.
3) Visualization of computed motions through image rendering and animation.

3-Dimensional Euler/N-S Aerodynamic Model

For computation of flowfields, CFD method considering both Euler and unsteady compressible Navier-Stokes equations was developed. Nondimensionalized Reynolds averaged Navier-Stokes equations in cartesian coordinate system are as follows.

$$\frac{\partial Q}{\partial t} + \frac{\partial E}{\partial x} + \frac{\partial F}{\partial y} + \frac{\partial G}{\partial z} = \frac{1}{Re_a}\left[\frac{\partial E_v}{\partial x} + \frac{\partial F_v}{\partial y} + \frac{\partial G_v}{\partial z}\right]$$

To increase numerical accuracy and efficiency, above equations are transformed to body fixed general curvilinear coordinate system (ξ, η, ζ). Here, ξ, η, ζ denote the chordwise, spanwise and normal direction, respectively. Transformed equations in strong conservation law form are as follows.

$$\frac{\partial \hat{Q}}{\partial t} + \frac{\partial \hat{E}}{\partial x} + \frac{\partial \hat{F}}{\partial y} + \frac{\partial \hat{G}}{\partial z} = \frac{1}{Re_a}\left[\frac{\partial \hat{E}_v}{\partial x} + \frac{\partial \hat{F}_v}{\partial y} + \frac{\partial \hat{G}_v}{\partial z}\right]$$

Here, conservative quantity vectors, and inviscid and viscous flux vectors are as follows.

$$\hat{Q} = \frac{1}{J} Q$$

$$\hat{E} = \frac{1}{J}[\xi_x E + \xi_y F + \xi_z G]$$
$$\hat{F} = \frac{1}{J}[\eta_x E + \eta_y F + \eta_z G]$$
$$\hat{G} = \frac{1}{J}[\zeta_x E + \zeta_y F + \zeta_z G]$$

$$\hat{E}_v = \frac{1}{J}[\xi_x E_v + \xi_y F_v + \xi_z G_v]$$
$$\hat{F}_v = \frac{1}{J}[\eta_x E_v + \eta_y F_v + \eta_z G_v]$$
$$\hat{G}_v = \frac{1}{J}[\zeta_x E_v + \zeta_y F_v + \zeta_z G_v]$$

Detailed explanation on transformation of governing equations and each element of matrix is in reference [10].

As numerical method for governing equation in the curvilinear coordinate system, FVM (Finite Volume Method) are used. For flux calculation, Roe's FDS upwind scheme is used to get accurate shock wave solution and viscous boundary layer. And MUSCL with Koren's limiter is used to get the 3rd order spatial accuracy. In time integration, the ADI scheme which has less limitation in time step or LU-SGS is used. In ADI integration method, jacobian of Van Leer FVS flux is used and in LU-SGS scheme, approximated jacobian is used to prevent matrix inversion. Equations resulted from LU-SGS method are as follows.

$$\left[I + \alpha\Delta t\left(-\frac{\partial A}{\partial \xi} + \frac{\partial B}{\partial \eta} + \frac{\partial C}{\partial \zeta}\right)\right]\Delta\hat{Q} = -\Delta t\hat{R}$$

$$LD^{-1}U\Delta\hat{Q} = -\Delta t\hat{R}$$

$$L = I + \alpha\Delta t(D^-_\xi A^+ + D^-_\eta B^+ + D^-_\zeta C^+ - A^- - B^- - C^-)$$
$$D = I + \alpha\Delta t(A^+ - A^- + B^+ - B^- + C^+ - C^-)$$
$$U = I + \alpha\Delta t(D^+_\xi A^- + D^+_\eta B^- + D^+_\zeta C^- + A^- + B^- + C^-)$$

Most of CFD codes determine the time step from CFL number, but in present method, time step is determined from rotation period, so we can easily exchange analysis data with the dynamic analysis part.

Grid System

Gird generation consists of initial grid generation and dynamic grid generation considering rotor blade motions. To construct initial grid, two-dimensional grid system around airfoil is constructed as C type using Inoue's conformal mapping,[28] and three dimensional grid system around rotating blade is constructed as C-H type by distributing two dimensional grid in spanwise direction. Fig. 1 shows grid system used in present analysis. Tip shape is assumed as bevelled tip, and satisfies surface orthogonality.

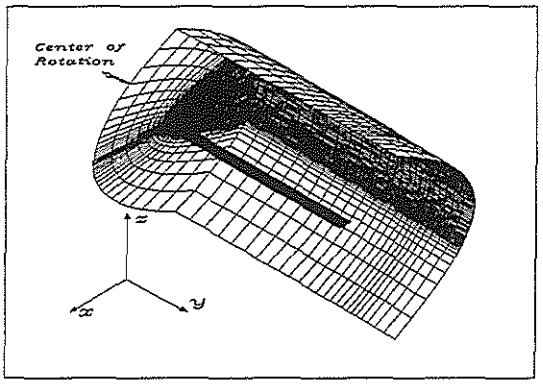

Fig. 1 Computational C-H type grid

Next, grid motion is considered in each time step. Motion of rotating blade is divided into rigid body motion and elastic body motion with respect to fixed coordinate system. To consider these, new grid system is generated in each time step by transformation matrix. Blade is divided in spanwise direction to consider geometrical nonlinearity, and constructing transformation matrix including flapping, pitching and torsion, and rotation and lead-lag motion for each element. And using these matrices, total transformation matrix is constructed by global/local coordinate transformation.

After new grid points are acquired, metric and jacobian are changed for computations. Generic metric terms are as follows.

$$\xi_t = J[x_t(y_\eta z_\zeta - y_\zeta z_\eta) + y_t(x_\zeta z_\eta - x_\eta z_\zeta) + z_t(x_\eta y_\zeta - x_\zeta y_\eta)]$$
$$\eta_t = J[x_t(y_\zeta z_\xi - y_\xi z_\zeta) + y_t(x_\xi z_\zeta - x_\zeta z_\xi) + z_t(x_\zeta y_\xi - x_\xi y_\zeta)]$$
$$\zeta_t = J[x_t(y_\xi z_\eta - y_\eta z_\xi) + y_t(x_\eta z_\xi - x_\xi z_\eta) + z_t(x_\xi y_\eta - x_\eta y_\xi)]$$

In above equations, x_t, y_t, z_t are calculated considering rotation, forward flight and velocities of pitch angle and blade deformations.

Wake Model

Momentum wake and prescribed wake model are used in present analysis. Momentum wake model is calculated by simple modified momentum theory, and considered constant along the span. In prescribed wake analysis, Landgrebe model is used,[33] and Kocurek and Tangler model[34] is also referred. In present analysis, the wake effect is incorporated into CFD code in the form of angle of attack correction, and the effects of the tip vortex and the wake effects within the computational domain are excluded.

Rotor Structural Model using ADAMS

For modelling and analysis on structural dynamics of rotor system, MDI's ADAMS package is used. ADAMS is used in multibody system analysis, such fields as automobile dynamics, aerospace engineering, electric engineering, human engineering and manufacturing. In present research, ADAMS installed on IRIS Indigo-2 workstation is applied to helicopter rotor system analysis.

Main feature of present analysis is the dynamic modelling of whole rotor system using multibody system modelling capability of ADAMS.[35,36] Fig. 2 shows modelling result of two-bladed rotor system. Modelled hub system is hingeless type, and the swashplate including rotating and nonrotating part has basic shape of general type. In hub system, main parts such as yoke, trunnion, grip and

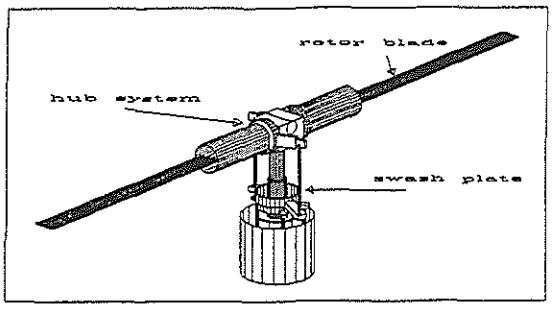

Fig. 2 Two-bladed rotor system modelling

pitch horn are modelled, and rotor blade is modelled as nonlinear beam for elastic motion and analysis. Besides, rotor shaft, pitch link, pitch control linkage, etc are also modelled. The modelled parts having six degrees of freedom are constrained by joints, so the rotor system motion is restricted to rotation, collective and cyclic pitch motion, and blade deformations. Rotation of rotor blade is controlled by modelled gear box, and pitch control is performed by nonrotating and rotating swashplate control. Helicopter fuselage is modelled by one rigid body for graphic visualization, and not considered in present analysis. In this paper, the result is limited in rotor blade, and whole system analysis is now being performed.

Numerical Procedure

Fig. 3 is flowchart of developed analysis method. In present method, the most important process is the exchange of aerodynamic loads and blade deformations between CFD code and ADAMS. To exchange aerodynamic forces at grid points of CFD code with ADAMS, spanwise grid points have the same number with beam model. And from pressure distribution computed for each spanwise element, forces and moments on the aerodynamic center are acquired, and these values are sent to aerodynamic control points of each beam element of ADAMS.

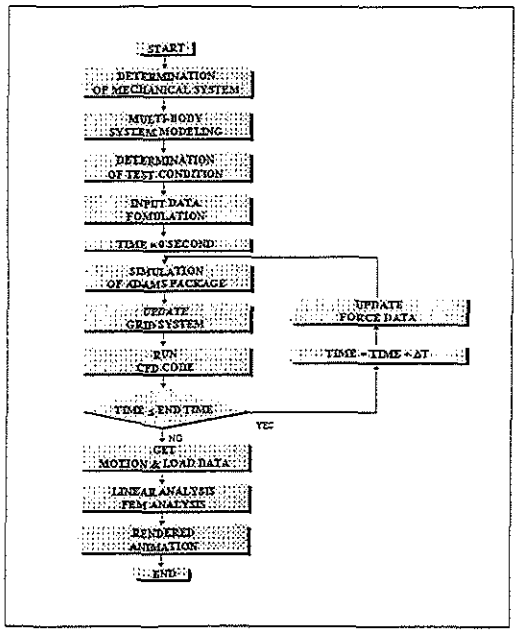

Fig. 3 Flowchart of present method

Here, aerodynamic control point is on the aerodynamic center at quarter chord, and the same process is performed to all blade elements. Blade deformations by aerodynamic forces, weight, inertia force and centrifugal force acting on aerodynamic control point, are calculated on each beam element, and these results are read by CFD code. And in CFD code, with regenerated dynamic grid system using blade deformation data, surface pressure distribution on grid points is re-obtained. And the process is repeated. So, between aerodynamic analysis module and structural dynamic analysis module, above data exchanging process is repeated by reading and writing data files.

After, These force and deformation solutions are converged, linear analysis to get modal frequency and damping results is performed, and rendering of graphic image is also given for realistic simulation of analysis.

Discussion of Results

Hover

A simplified rotor blade with an untwisted rectangular planform is used in the present analysis to investigate the effect of developed aeroelastic analysis method. Mass and stiffness properties along the blade span are assumed to be constant. The chordwise offsets of mass, tension, and aerodynamic center from the elastic axis are also considered to be zero. Table 1 is some of the rotor configuration and operation parameters used in this calculation.

The unsteady Euler calculations are all done on a 121×21×30 grid with 79 points on the airfoil and 15 span stations, and verified with experimental results.[37] The dimensionless time step $\Delta\Psi$ is 5° and there is 10 ~ 100 steps in CFD computations. In the following result of deformations, the bending deflections in the flap and lead-lag directions are normalized with respect to the blade radius, and the torsional deflection is given in degrees.

Fig. 4 shows the result of flexible rotor blade modelling of present analysis. It is shown that the rotor blade is deformed by aerodynamic loads compared with initial blade. Convergency results of tip deflections with azimuth are shown on fig. 5. In this case, analysis requires only three revolutions to converge for steady state solutions of the deformed blade, so present method needs much less computation time than supposed.

Fig. 6 shows equilibrium flap deflections at the blade tip for two- and four-bladed stiff-inplane rotors with momentum wake model. Note that as the number of blades increases, the deflections decrease because of reduction in wake effect. Compared with the results of camrad/ja analysis, it is observed that two case have similar trend, but more accurate consideration of three dimensional effect by present method, the lower tip deflection is obtained. Four-bladed rotor tip

Parameter	Value
chord (m)	0.3
span (m)	5.0
cutout	0.2
number of blade	2, 4
rotation speed (rad/sec)	43.6
flap stiffness ($N \cdot m^2$)	8.317E4
lag stiffness ($N \cdot m^2$)	1.248E6
torsion stiffness ($N \cdot m^2$)	4.159E4

Table 1 Rotor blade parameters

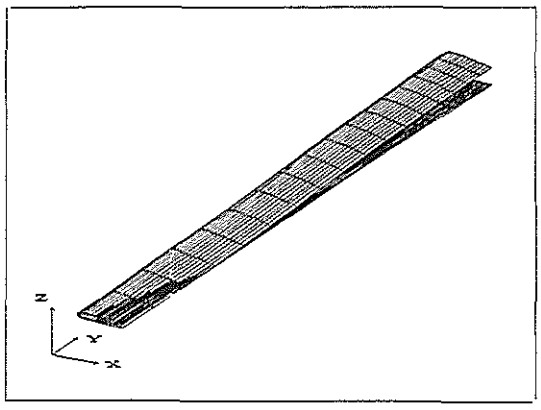

Fig. 4 Deflection of elastic blade model

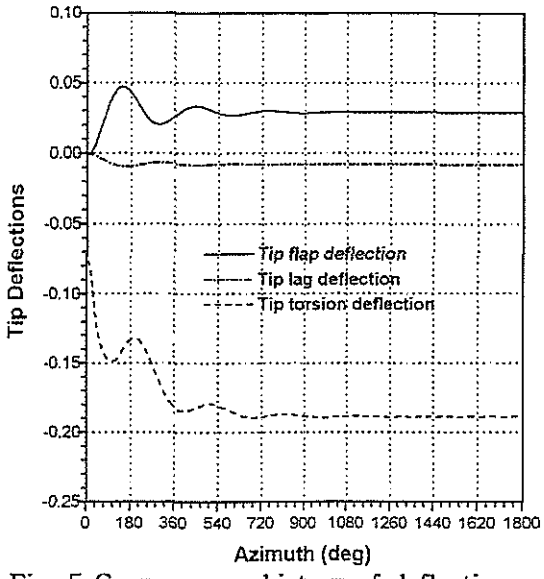

Fig. 5 Convergency history of deflections

flap and lag deflection for momentum and prescribed wake model are compared in fig 7. In analysis with prescribed wake model,

the tip vortex effects are more likely to be captured. The impact of these effect should be felt at the higher collective pitch where the flowfields become more complex. Fig. 8 shows fundamental lag frequencies with various lag stiffness. Nondimensional lag stiffness has the value of 0.01, 0..5, 0.1, 0.15, 0.2, and it is shown that lag frequency varies from the value less than 1/rev of soft inplane rotor to the value of stiff inplane rotor. Tip lag deflections in same case are given in fig. 9. It is verified that the lag deflection decreases with the increase of nondimensional lag stiffness.

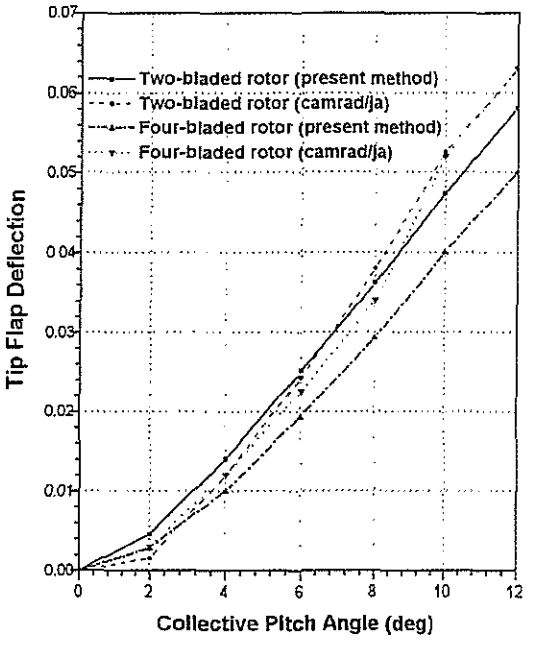

Fig. 6 Equilibrium tip flap deflection

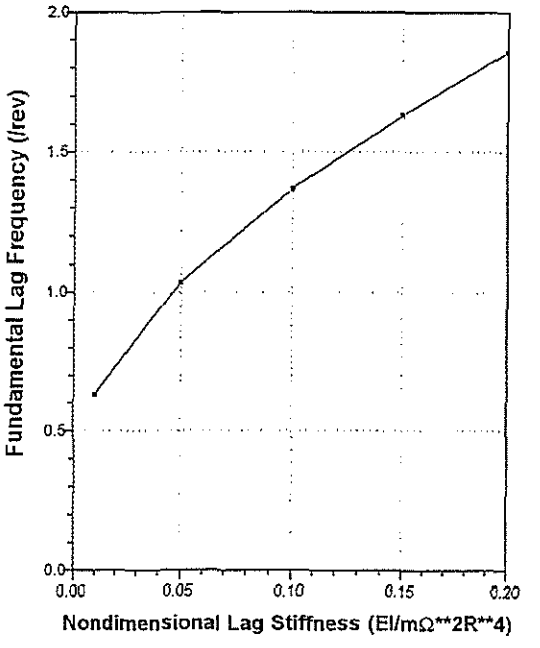

Fig. 8 Effect of lag stiffness on frequency

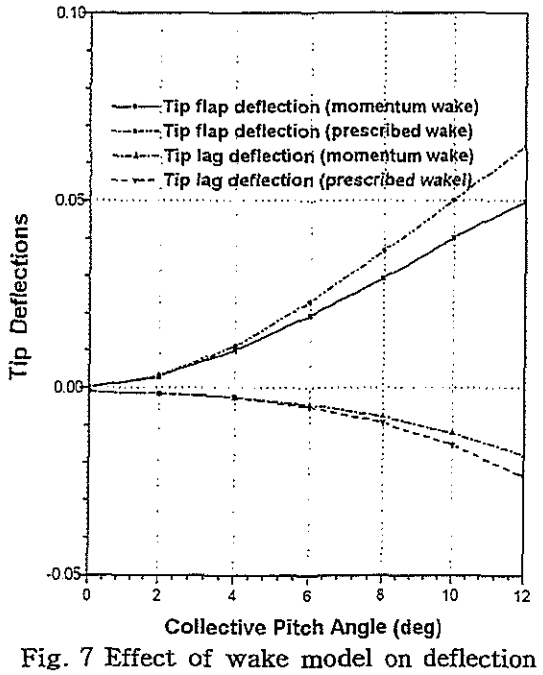

Fig. 7 Effect of wake model on deflection (Four-bladed rotor, collective pitch angle 8°)

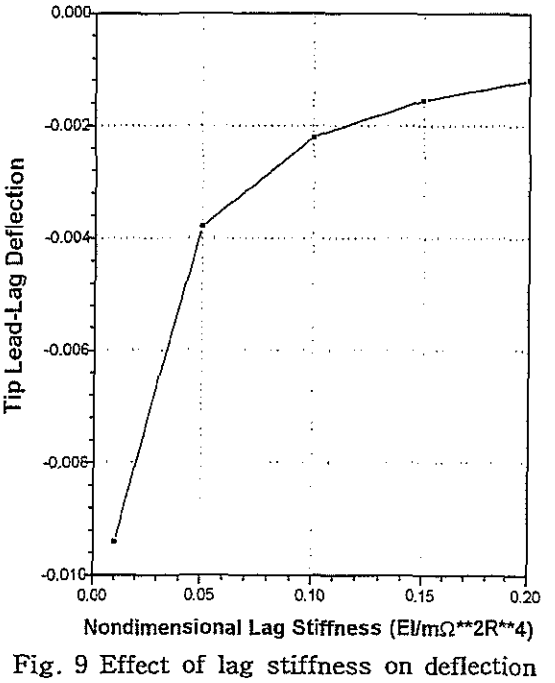

Fig. 9 Effect of lag stiffness on deflection

Forward Flight

Forward flight analysis is performed using the same blade parameters, but the lag stiffness is changed to the property of soft inplane rotor. Rotation speed is set to 40.123 rad/sec, and advance ratio is selected as 0.3. The collective and cyclic control pitch results are obtained from trim analysis module, Fig. 10 shows periodic change of pitch angle, and it is shown that minimum pitch angle is occurred at advancing side and maximum pitch angle is at retreating side. Thrust coefficients of rigid and elastic blade model are compared in fig. 11. From this figure, the elastically modelled blade gives much more balanced thrust distribution due to the considering of flapping motion. So elastic blade assumption is necessary to get more realistic results of flowfields analysis. Fig. 12 shows blade deformations including flapping, lag, and torsion with azimuth. Comparing graph on thrust and flapping, it is verified that the phase lag between maximum flapping position and maximum thrust position is about 90°. Fig. 13 shows thrust contour, and the longitudinally and laterally balanced thrust distribution is given. Fig. 14 shows graphic modelling of two-bladed rotor system including fuselage, and fig. 15 is rendered image of rotor system. Numerical simulation of rotor motion is presented in fig. 16, and it is shown that rotor blade is deformed by forces.

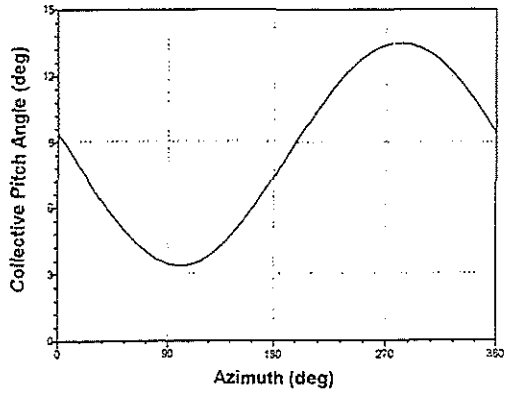

Fig. 10 Pitch angle variation

($\mu = 0.3,\ \theta = 8.4^\circ + 1^\circ\cos\psi - 4.9^\circ\sin\psi,\ \alpha_s = 6.13^\circ$)

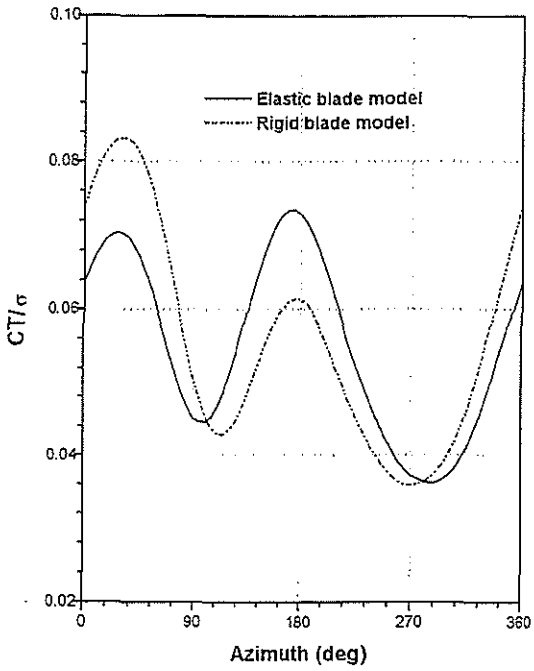

Fig. 11 Comparison of C_T/σ

($\mu = 0.3,\ \theta = 8.4^\circ + 1^\circ\cos\psi - 4.9^\circ\sin\psi,\ \alpha_s = 6.13^\circ$)

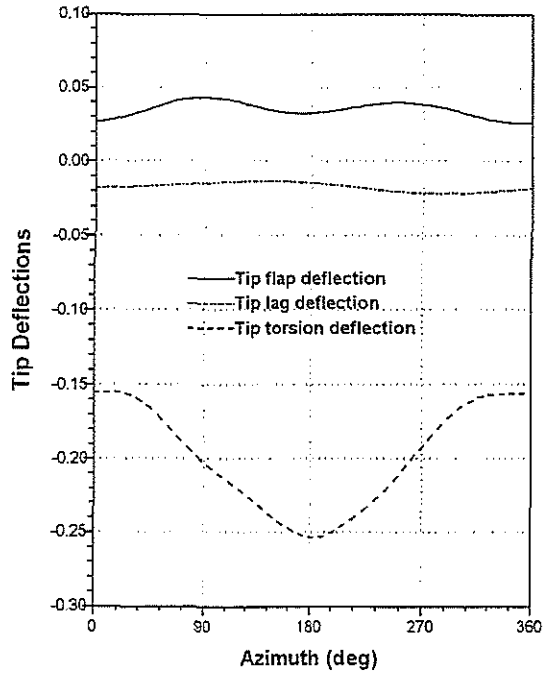

Fig. 12 Blade deformations in forward flight

($\mu = 0.3,\ \theta = 8.4^\circ + 1^\circ\cos\psi - 4.9^\circ\sin\psi,\ \alpha_s = 6.13^\circ$)

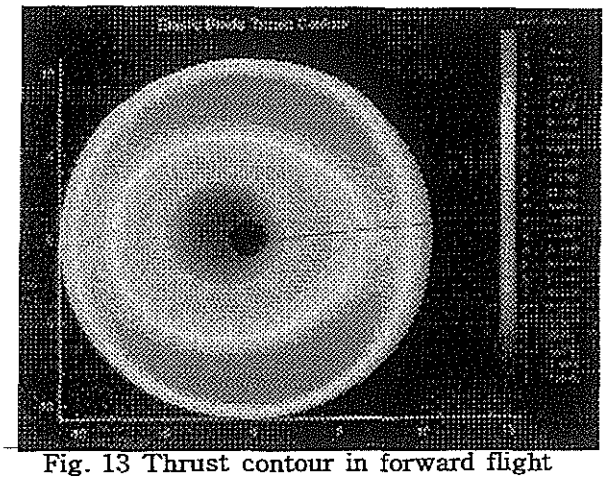

Fig. 13 Thrust contour in forward flight
($\mu = 0.3$, $\theta = 8.4^\circ + 1^\circ\cos\psi - 4.9^\circ\sin\psi$, $\alpha_s = 6.13^\circ$)

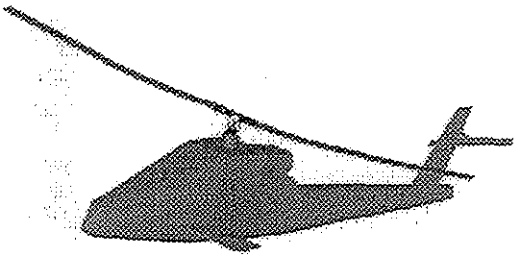

Fig. 16 Numerical simulation of helicopter rotor motion

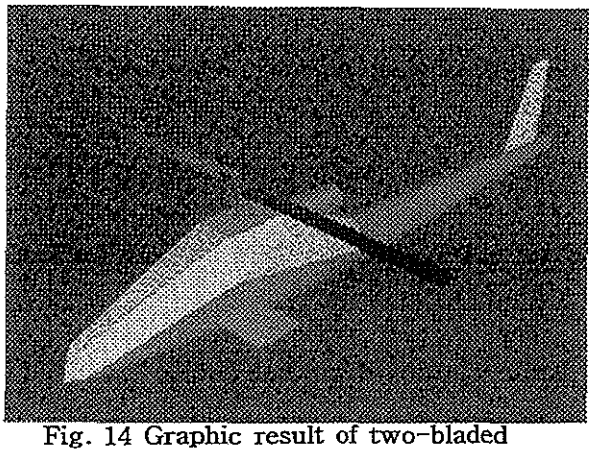

Fig. 14 Graphic result of two-bladed helicopter

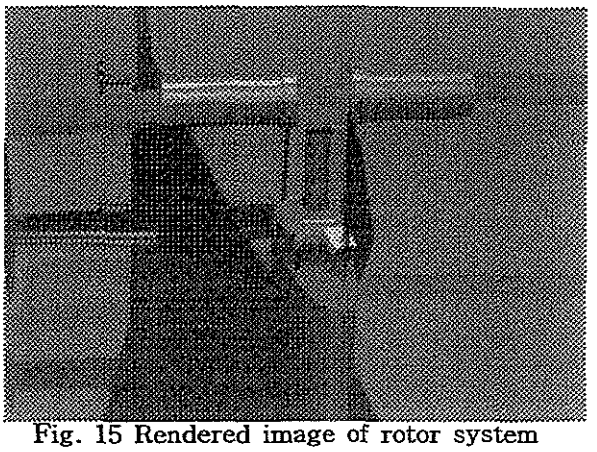

Fig. 15 Rendered image of rotor system

Conclusions

Comprehensive aeroelastic analysis method with elastic rotor blade model has been developed for multibody system modelling and aeroelastic analysis of rotor system in hover and forward flight.

In present method, a more realistic analysis of flowfields using aerodynamic model based on Euler/Navier-Stokes solver, and elastic motion analysis with beam modelled rotor blade are included. Modelling and analysis of whole rotor system including rotor blade, rotor hub, and swashplate system are also possible.

Using developed method, aeroelastic analysis has been performed in hover and forward flight changing lag stiffness, thus aerodynamic loads, blade deformations, stability characteristics, and graphic animation of rotor motions are obtained. Compared with the analysis using rigid blade modelling and proven method, it is found that more realistic solutions are obtained for the aerodynamic loads and blade deformations in present method. The results show that the effect of elastic blade motion and three dimensional aerodynamic loads are important in analysis of flowfields and dynamic characteristics of rotor system.

References

[1]R. K. Agarwal, J. E. Deese, "Euler Calculations for Flow Field of a Helicopter Rotor in Hover," Journal of Aircraft, Vol.24, No.4, pp. 231-238, 1987

[2]B. E. Wake, N. L. Sankar, S. G. Lekoudis, "Computation of Rotor Blade Flows Using the Euler Equations," Journal of Aircraft, Vol.23, No.7, pp. 582-588, 1988

[3]B. E. Wake, N. L. Sankar, "Solutions of the Navier-Stokes Equations for the Flow about a Rotor Blade," Journal of AHS, pp. 13-23, 1989

[4]G. R. Srinivasan, etc, "Flowfield of a Lifting Rotor in Hover: A Navier-Stokes Simulation," AIAA Journal, Vol.30, No.10, pp. 2371-2378, 1992

[5]K. R. Shenoy, "A Method of Computing the Pressure Distribution on a Single-Bladed Hovering Helicopter Rotor," Georgia Institute of Technology, Feb 1979

[6]I. C. Chang, "Transonic Flow Analysis for Rotors," NASA-TP 2375, 1990

[7]E. Kramer, S. Hertel, S. Wagner, "Euler Procedure for Calculations of Hovering Rotor Flowfields," Journal of Aircraft, Vol.25, No.10, pp. 865-874, 1988

[8]C. J. Chen, W. J. McCroskey, "Numerical Solutions of the Forward-Flight Rotor Flow Using an Upwind Method," Journal of Aircraft, Vol. 28, No. 6, June, 1991, pp. 374-380

[9]D. Lee, S. Kim, "An Efficient Method to Calculate Rotor Flow in Hover & Forward Flight," 18th AIAA Computational Fluid Dynamics Conference, Orlando, FL, July 6-9, 1993

[10]C. Nam, D. Lee, "Navier-Stokes Calculation of Rotating BERP Planform Blade Flowfields," AIAA Applied Aerodynamics Conference, Montery, CA, August 9-11, 1993

[11]E. P. N. Duque, G. R. Srinivasan, "Numerical Simulation of A Hovering Rotor Using Embedded Grids," AHS 48th Annual Forum and Technology Display, June 3-5, 1992

[12]D. L. Sharpe, "An Experimental Investigation of Flap-Lag-Torsion Aeroelastic Stability of the Small-Scaled Hingeless Helicopter Rotor in Hover," NASA TP 2546, AVSCOM Technical Report 85-A-9, Jan., 1986

[13]W. G. Bousman, D. L. Sharpe, R. A. Ormiston, "An Experimental Study of Techniques for Increasing the Lead-Lag Damping of Soft Inplane Hingeless Rotor," 32nd Annual National V/STOL Forum of the AHS, May, 1976

[14]R. L. Peterson, W. Warmbrodt, "Hover Performance and Dynamics of Full-Scale Hingeless Rotor," Journal of American Helicopter Society, pp. 10-18, July, 1986

[15]S. Dawson, "An Experimental Investigation of the Stability of Bearingless Model in Hover," Journal of the American Helicopter Society, pp. 29-34, Oct., 1983

[16]G. H. Gaonkar, M. J. Mcnulty, "An Experimental and Analytical Investigation of Isolated Rotor Flap-Lag Stability in Forward Flight," 11th European Rotorcraft Forum, Paper No. 66, Sep., 1985

[17]R. A. Ormiston, "Investigation of Hingeless Rotor Stability," Vertica, Vol.7, No.2, pp. 143-181, 1983

[18]O. J. Kwon, "A Technique for the Prediction of Aerodynamics and Aeroelasticity of Rotor Blades," Georgia Institute of Technology, Nov 1988

[19]G. Bir, I. Chopra, "Status of University of Maryland Advanced Rotorcraft Code (UMARC)," AHS Aeromechanics Specialists Conference, San Francisco, CA, Jan. 19-21, 1994

[20]W. B. Stephan, M. J. Rutkowski, R. A. Orimston, C. M. Tan, "Development of the Second Generation Comprehensive Helicopter Analysis System (2GCHAS)," Proceedings of the National Specialists' Meeting on Rotorcraft Dynamics, American Helicopter Society, Arlington, Texas, November, 1989

[21]N. T. Sivaneri, I. Chopra, "Finite Element Analysis for Bearingless Rotor Blade

Aeroelasticity," Journal of the American Helicopter Society, Vol. 29, No. 2, April, 1984
[22]N. T. Sivaneri, I. Chopra, "Dynamic Stability of a Rotor Blade Using Finite Element Analysis," AIAA Journal, Vol. 20, No. 5, May, 1982
[23]E. C. Smith, I. Chopra, "Aeroelastic Response, Loads, and Stability of a Composite Rotor in Forward Flight," AIAA journal, Vol.31, No.7, July, 1993
[24]A. R. Manjunath, etc, "Flap-Lag Damping in Hover and Forward Flight With a Three-Dimensional Wake," Journal of AHS, oct., 1993
[25]T. H. Maier, D. L. Sharpe, J. W. Lim, "Fundamental Investigation of Hingeless Rotor Aeroelastic Stability, Test Data and Correlation," AHS 51st Annual Forum, May 9-11, 1995
[26]M. H. Cho, I. Lee, "Aeroelastic Analysis of Multibladed Hingeless Rotors in Hover," AIAA Journal Vol. 33, No. 12, Dec 1995
[27]M. J. Smith, D.H. Hodges, "Development of an Aeroelastic Method for Hovering Rotors with Euler/Navier-Stokes Aerodynamics," AHS 51st Annual Forum, May 9-11, 1995
[28]K. Inoue, "Grid Generation for Single Airfoil using Conformal Mapping, "NALTR-851T
[29]T. L. Thompson, "Velocity Measurements for the Blade Tip and in the Tip Vortex Core of a Hovering Model Rotor," Georgia Institute of Technology, december, 1986
[30]C. He, "Development and Application of a Generalized Dynamic Wake Theory for Lifting Rotors," Georgia Institute of Technology, July, 1989
[31]R. B. Gray, "Vortex Modeling for Rotor Aerodynamics-The 1991 Alexander A. Nikolsky Lecture," 47th Annual Forum of the AHS, Phoenix, AZ, May 1991
[32]A. Su, K. M. Yoo, D. A. Peters, "Extension and Validation of an Unsteady Wake Model for Rotors," Journal of Aircraft, Vol. 29, No. 3, May-June 1992
[33]A. J. Landgrebe, "The Wake Geometry of a Hovering Helicopter Rotor and Its Influence on Rotor Performance," Proceedings of the 28th Annual Forum of AHS, 1972
[34]J. D. Kocurek, J. L. Tangler, "A Prescribed Wake Lifting Surface Hover Performance Analysis," Journal of AHS, Vol. 22, No. 1, 1977
[35]D. Lee, B. Ahn, K. Yee, "Numerical Experiment of a Helicopter Driving System By Using ADAMS Code," 5th AIAA/USAF/NASA/ISSMO Symposium on Multidisciplinary Analysis and Optimization, September 7-9, 1994
[36]O. A. Bauchau, N. K. Kang, "A Multibody Formulation for Helicopter Structural Dynamic Analysis," Journal of AHS, April, 1993
[37]F. X. Caradonna, C. Tung, "Experimental and Analytical Studies of a Model Helicopter Rotor in Hover," NASA TM 81232, 1980
[38]Wayne Johnson, "A Comprehensive Analytical Model of Rotorcraft Aerodynamics and Dynamics," NASA TM-811182, 1982